NJC

ROYAL SOCIETY OF CHEMISTRY

PAPER

View Article Online
View Journal

Cite this: DOI: 10.1039/d5nj02110c

Gold(III) complexes containing (non)protonated oligopyridines—unexpected results in cancer drug research†

Kseniya A. Koshenskova,[a] Elena E. Bardina,[b] Eugeniya V. Makotchenko,[b] Viktoria Yu. Kharlamova,[b] Igor V. Mironov,[b] Olga B. Bekker,[c] Helen M. Treshalina,[d] Darina V. Sokolova,[d] Vadim S. Pokrovsky,[de] Eugenii A. Borodin,[f] Danil D. Kotel'nikov,[f] Danila V. Belyaev,[gh] Diana V. Vakhrusheva,[g] Svetlana Yu. Krasnoborova,[g] Gennadii L. Rusinov,[gh] Eduard A. Timofeev,[i] Nataliya Yu. Leusova,[i] Mikhail A. Kiskin,[a] Artem L. Gushchin,*[b] Igor L. Eremenko[a] and Irina A. Lutsenko*[ae]

Received 19th May 2025,
Accepted 16th July 2025

DOI: 10.1039/d5nj02110c

rsc.li/njc

Two novel gold(III) complexes with doubly protonated forms of phenanthrolines, $(neocH_2)[AuCl_4]\cdot Cl$ (**1**) and $(1,7\text{-}phenH_2)[AuCl_4]\cdot NO_3$ (**2**), were synthesized using the oligopyridines 2,9-dimethyl-1,10-phenanthroline (neocuproine, neoc) and 1,7-phenanthroline (1,7-phen). The structures of the compounds were established using single-crystal X-ray diffraction analysis. In crystals **1** and **2**, the tetrachloroaurate anions form a whole network of various non-covalent interactions with protonated forms of oligopyridines ($neocH_2^{2+}$, $neocH^+$, $1,7\text{-}phenH_2^{2+}$) and Cl^-/NO_3^- anions (N/C–H···Cl, N–H···O, Au···π, Au–C···π, π···π). A comparative study of the stability of complexes **1** and **2**, as well as complexes with coordinated oligopyridines, *i.e.*, $[Au(neoc)Cl_3]$ (**1a**), $[Au(1,7\text{-}phen)Cl_3]$ (**2a**), $[Au(1,10\text{-}phen)Cl_2]PF_6$ (**3**, 1,10-phen is 1,10-phenanthroline) and $[Au(bpy)Cl_2]PF_6$ (**4**, bpy is 2,2′-bipyridine), was carried out in DMSO and aqueous solutions. When complexes **1a**, **2a**, **3**, and **4** were tested with glutathione (GSH) under near-physiological conditions, they formed gold(I) complexes of the type $[Au(GSH)_2]^{3-}$. The *in vitro* biological activities of the complexes were determined against mycobacterial strains (*Mycolicibacterium smegmatis* and *Mycobacterium tuberculosis H37Rv*) and a number of test cancer lines. A high level of selective activity was detected for **1** in relation to a non-cancerous human fibroblast culture – the selectivity index (SI) was 371 compared to the cancer cell line HCT116. Molecular docking studies showed that compound **1** forms protein–gold supramolecular complexes with high affinity and stability.

Introduction

Metal-containing drugs, primarily platinum-containing ones that show high anticancer efficacy, are widely used in medicine. However, in the past two decades, chemists, biologists, physicians, and other researchers started focusing their efforts on the development of synthetic approaches and various types of biological research involving "non-platinum" antitumor agents

[a] N.S. Kurnakov Institute of General and Inorganic Chemistry of the Russian Academy of Sciences, Leninsky Prosp. 31, 119991 GSP-1 Moscow, Russian Federation. E-mail: irinalu05@rambler.ru; Fax: +7(495) 952 1279
[b] A. V. Nikolaev Institute of Inorganic Chemistry, Siberian Branch of Russian Academy of Sciences, Acad. Lavrentiev Ave., 3, Novosibirsk, 630090, Russian Federation. E-mail: gushchin@niic.nsc.ru
[c] N. I. Vavilov Institute of General Genetics, Russian Academy of Sciences, Gubkina, 3, 119333, Moscow, Russian Federation
[d] Federal State Budgetary Institution "N. N. Blokhin National Medical Research Center of Oncology" of the Ministry of Health of the Russion Federation, Kashirskoe Shosse, 24, Moscow, 115478, Russian Federation
[e] RUDN University, Miklukho-Maklaya 6, Moscow, 117198, Russian Federation
[f] Amur State Medical Academy, Ministry of Health of the Russian Federation, Gorkogo str., 95, Blagoveshchensk, 675001, Russian Federation
[g] National Medical Research Center of Phthisiopulmononlogy and Infectious Diseases of Ministry of Health of the Russian Federation, 22nd Partsyezda str., 50, Ekaterinburg, 620039, Russian Federation
[h] I. Ya. Postovsky Institute of Organic Synthesis of the Ural Branch of the Russian Academy of Sciences, S. Kovalevskoy Str., 22, Ekaterinburg 620137, Russian Federation
[i] Institute of Geology and Nature Management, Far Eastern Branch, Russian Academy of Sciences, per. Relochnyi, 3, Blagoveshchensk, 675000, Russian Federation

† Electronic supplementary information (ESI) available. CCDC 2330029 (**1**) and 2330030 (**2**). For ESI and crystallographic data in CIF or other electronic format see DOI: https://doi.org/10.1039/d5nj02110c

based on both bio-essential (vital) metals, *e.g.*, Cu, Zn, Fe, and Co, and metals with potential biological activity, such as Ag, Ru, and Au.[1–5] This shift in researchers' focus is due to numerous reasons: first, the search for cheaper drugs; and second, the need to reduce the toxicity of drugs that concurrently act on multiple targets. It should be noted that the interest in the antimicrobial properties of gold is not new. Gold, in its variety of forms, has been used in medicine throughout the history of civilization, from the archaic ''elixir of life, cinnabar'' to quite real therapeutic agents, for example, those intended for the treatment of rheumatoid arthritis (gold thiolates, auranofin).[6–8] As early as the late 19th century, Robert Koch began using potassium dicyanoaurate(I), $K[Au(CN)_2]$, to treat tuberculosis. Since then, interest in the anti-infective activity of gold complexes has grown and the range of bacteria, fungi, and parasites being studied has expanded. In addition, studies of Au-based compounds that feature efficient antiproliferative (aimed at suppressing excessive cell proliferation) and antiangiogenic properties are increasingly relevant.[9–13] It was in the 20th century that the use of radioactive gold-198 in antitumor therapy began: it is chemically inert, inhibits the formation of intracavitary fluid, and has a relatively short half-life (2–7 days).[14] In the compounds both Au(III) and Pt(II) are isoelectronic with a d^8 configuration, which favours the formation of square-planar complexes and results in relatively slow ligand exchange kinetics—a feature that underpins the development and testing of gold-based complexes as potential anticancer drugs. Gold complexes with phosphine ligands have been studied most thoroughly regarding their antiproliferative properties.[15–22] Of no less importance in recent years have been studies on compounds that contain chelating N-ligands (oligopyridines such as bipyridines and phenanthrolines). For example, S. Carotti *et al.*[23–25] studied gold(III) complexes with various N-donor ligands and found that these compounds exhibit stability under physiological conditions, show high cytotoxic activity against ovarian cancer cells (A2780) and can overcome resistance phenomena. An interesting and promising aspect is that the compounds simultaneously exhibit multidirectional biological effects, for example, cytostatic and antibacterial activity. The ability to activate different targets and hence different mechanisms of action (so-called multi-target agents) certainly opens up broader prospects for new compounds as drug candidates. Gold complexes can become leaders in this area (following the essential metal Cu[5,26–28]), as the metal centre itself is characterized by high antitumor activity (it features a high affinity for thiol-containing enzymes such as thioredoxin reductase, glutathione reductase, and cysteine protease),[29] and, moreover, ligands coordinated to gold are capable of exhibiting chemoprotective effects. However, all published gold(I,III) complexes with oligopyridines are coordination compounds in which N-donors are covalently bound to the metal centre. In this work, we tried to evaluate the cytotoxic activities of complexes in which the ligand is in a doubly protonated form and is not coordinated to gold. To obtain a complete picture of the ''structure–bioactivity'' relationship, we were able to obtain previously published compounds (with coordinated oligopyridines) and compare their physicochemical and biological properties with the new compounds.[30–33] This work presents the synthesis of gold(III) complexes with 2,9-dimethyl-1,10-phenanthroline (neoc) and 1,7-phenanthroline (1,7-phen) under different reaction conditions. Their structures were determined, their stability in solution was evaluated, and their interactions with glutathione (GSH) were examined. The *in vitro* biological activity of these compounds against the mycobacterial strains *Mycolicibacterium smegmatis* and *Mycobacterium tuberculosis* (H37Rv), as well as their antiblastoma activity against human breast adenocarcinoma (SKBR3), human colorectal adenocarcinoma (HCT116), and human lung carcinoma (A549) were evaluated.

Results and discussion

Synthesis and structural characterization of 1 and 2

In contrast to previously reported[11,30–33] Au(III) complexes with various oligopyridines (such as 1,10-phen, neoc, bpy) that were synthesized in non-aqueous or mixed aqueous/organic solutions, the use of strongly acidic solutions results in a different binding pattern. Under these conditions, protonation of the nitrogen atoms of the N-donor ligands blocks the coordination to the gold centre. Therefore, the resulting complexes **1** and **2** are ionic compounds in which the tetrachloroaurate anion interacts through hydrogen bonds with the doubly protonated phenanthroline ligands (Scheme 1). According to single-crystal X-ray diffraction studies, complexes **1** and **2** belong to the triclinic system (the crystallographic parameters and X-ray diffraction experimental parameters are given in Table S1, ESI†). A crystal of **1** contains $neocH_2^{2+}$ and $neocH^+$ cations, a pair of $AuCl_4^-$ anions occupying two independent positions, and one chloride anion. The structural elements are packed into a crystal due to intermolecular non-covalent coupling. Alternating $neocH_2$ molecules and chlorine atoms form a 1D chain along the 0*b* axis due to N/C–H···Cl contacts (Fig. 1a and Table 1).

The chain pairs are connected to each other through interactions between the proton of the methyl group in $neocH_2$ and the chlorine atom (Table 1), resulting in the formation of a supramolecular layer $\{(neocH_2)^{2+}Cl\}_n$ with a corrugated shape due to the aromatic molecules being displaced from the center (Fig. 1b).

The aromatic moieties on each side of the layer are strengthened by additional Au···π (3.479, 3.633 Å) and Au–Cl···π interactions (Table 2) formed by $AuCl_4^-$ anions and benzene or pyridyl rings (Fig. 1c). The layers described above are surrounded on both sides by stacks formed through of π···π-interactions between $neocH^+$ cations (Fig. 1d and Table 3), with $AuCl_4^-$ anions linked to them *via* C–H···Cl interactions. The stacks of $\{(neocH)(AuCl_4)\}$ and layers of $\{(neocH_2)Cl(AuCl_4)\}$ are connected to each other through C–H···Cl interactions (Fig. 1e, f and Table 1). A crystal of **2** consists of $1,7\text{-}phenH_2^{2+}$ dications and $AuCl_4^-$ and NO_3^- anions that are connected to each other by a network of non-covalent interactions (Fig. 2a). The $1,7\text{-}phenH_2^{2+}$ cations form a pair of N–H···O bonds with nitrate anions, resulting in the formation of a supramolecular chain $\{(1,7\text{-}phenH_2)NO_3\}_n$ (Fig. 2b and Table 1). The adjacent chains

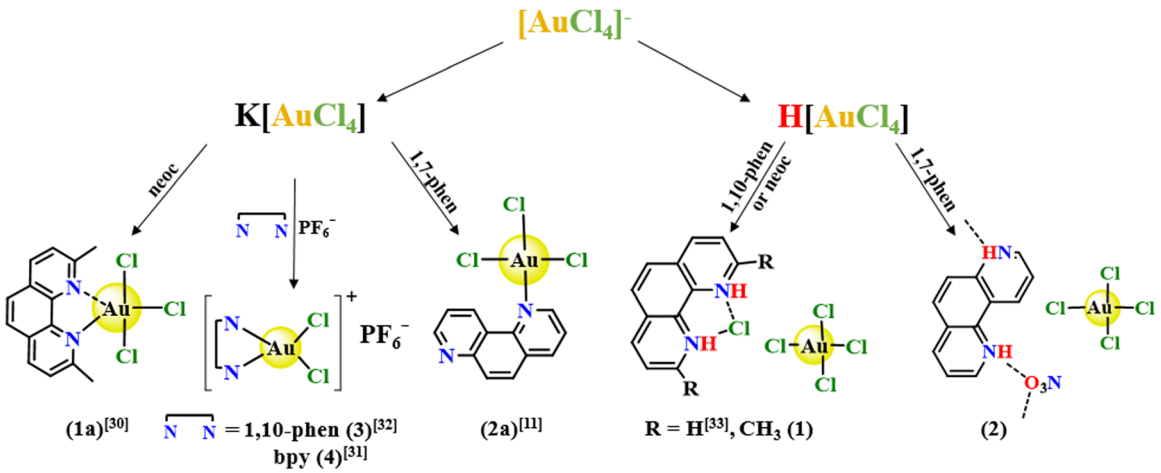

Scheme 1 Synthetic routes to compounds **1–4**.

contact each other through N–O···π interactions to form a layer (Fig. 2c and Table 2). The C–H···Cl and Au–Cl···π interactions (Tables 1–3) between the 1,7-phenH_2^{2+} dications of the supramolecular layer and the $AuCl_4^-$ anions connect the crystal lattice elements into a three-dimensional network (Fig. 2d).

Thus, the crystal packing of **1** consists of $\{(neocH_2)Cl(AuCl_4)\}_n$ supramolecular layers and $\{(neocH)(AuCl_4)\}$ stacks held together by intermolecular interactions. In crystal **2**, the $\{(1,7\text{-phen}H_2)NO_3\}_n$ supramolecular layers are non-covalently linked by $AuCl_4^-$ anions into a continuous network.

Stability in solutions

A comparative study of the stabilities of both compounds **1** and **2** and complexes with coordinated moieties of oligopyridines, *e.g.*, [Au(neoc)Cl_3] (**1a**), [Au(1,7-phen)Cl_3] (**2a**), [Au(1,10-phen)Cl_2]PF_6 (**3**), and [Au(bpy)Cl_2]PF_6 (**4**) (Scheme 2), the synthesis and structures of which were previously reported,[11,30–32] was carried out in various solutions.

In contrast to complexes **3** and **4**, in which the N-donor heterocycle (1,10-phen or bpy) is coordinated to the Au(III) ion in a symmetrical bidentate cyclic manner, asymmetric coordination of the neoc heterocycle is observed in complex **1a** (the Au–N1 and Au–N2 distances are 2.09 and 2.58 Å, respectively). In this case, the coordination environment of Au(III) consists of three Cl atoms and two N atoms; the coordination type is {4+1}. The difference between the symmetric coordination of 1,10-phen in **3** and the asymmetric coordination of neoc in **1a** appears to be due to steric hindrance owing to the methyl groups of neoc in close proximity to the coordination site. However, the symmetric bidentate coordination of neoc is still known: it is realized in the binuclear complex $[Au_2(\mu_2\text{-}O)(neoc)_2]^{2+}$ (similar Au–N bond lengths: 2.057 and 2.071 Å).[34,35] Complex **2a** includes a 1,7-phen heterocycle coordinated in a monodentate way to Au(III), as the arrangement of nitrogen atoms precludes a chelating coordination mode.

Stability in DMSO

To study the behaviours of complexes **1–4** in DMSO, ^{1}H NMR spectroscopy in DMSO-d_6 (99.9%) was used. To our knowledge, similar studies have not been conducted for the previously described compounds **1a**, **2a**, **3** and **4**. The spectra were recorded initially and also at the following times: 24, 48 and 72 h. The ^{1}H NMR spectrum of a freshly prepared solution of complex **1** in DMSO-d_6 contains four peaks corresponding to the four types of C–H protons in the structure of doubly protonated neoc ($neocH_2^{2+}$) (Table S2 and Fig. S1, ESI†). The signals are shifted downfield compared to non-protonated neoc. No spectral changes were detected over the time scale used, indicating that **1** was stable in DMSO for at least 72 h, although we cannot exclude the replacement of Cl^- by DMSO in the $[AuCl_4]^-$ anion, which would not affect the position of signals from the $neocH_2^{2+}$ cation significantly. Note that the synthesis of $[Au(DMSO)_2Cl_2]Cl$ from $K[AuCl_4]$ was reported earlier.[36] The ^{1}H NMR spectrum of a solution of complex **1a** initially contains a set of four signals shifted downfield relative to uncoordinated neoc (Table S3 and Fig. S2, ESI†). (Given the asymmetrical arrangement of the neoc ligand in structure **1a**, a set of eight peaks should be expected due to the non-equivalence of all protons). A similar spectrum of four lines was also observed when less-polar $CDCl_3$ was used instead of DMSO-d_6. This behaviour can be attributed to a dynamic process in the solution, wherein the Au(III) ion binds to either one or the other nitrogen atom of the heterocycle, which results in the averaging of the signals (Scheme 3).

A similar picture was observed previously for a series of Au(I) complexes with asymmetrically coordinated diimine ligands.[37] The ^{1}H NMR spectrum of complex **1a** evolves over time. After 24 h, a new set of four signals appears in the spectrum. This is most likely due to the substitution of Cl^- by DMSO, and the formation of the mixed DMSO/Cl complex **1a′**. Complete conversion of **1a** to **1a′** occurs after 72 h. The ^{1}H NMR spectrum of complex **2a** contains eight signals that correspond to the eight non-equivalent protons of 1,7-phen coordinated in a monodentate way (Table S4 and Fig. S3, ESI†). The spectrum does not evolve over time, indicating that **2a** is stable in DMSO for at least 144 h. Conversely, it cannot be excluded that **2a** rapidly reacts with DMSO, and the spectrum observed at the initial moment of time already corresponds to a form involving a

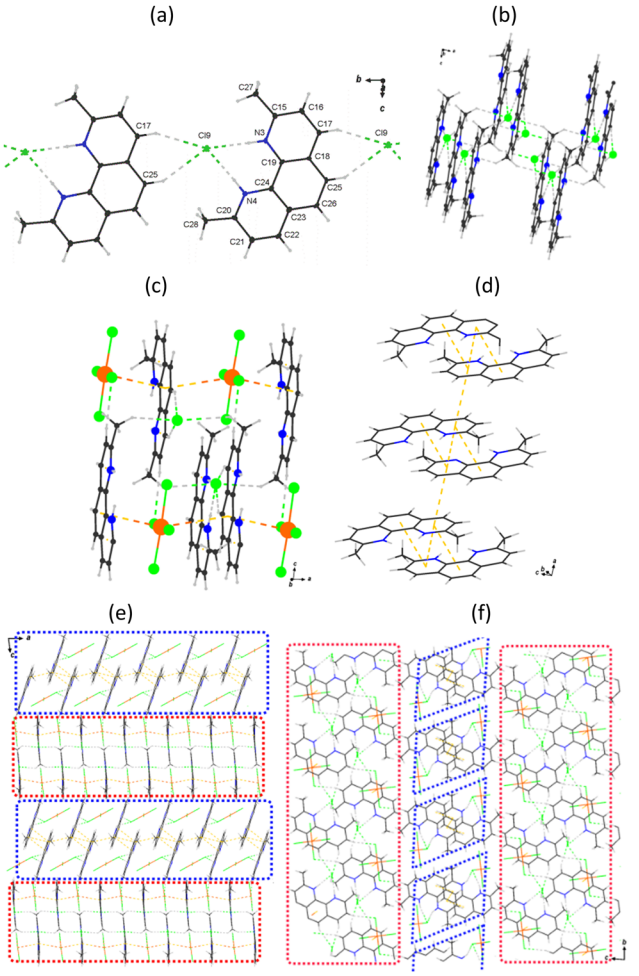

Fig. 1 Fragments of packing for **1**: (a) the packing of $neocH_2$ cations and Cl^- anions into a supramolecular chain (thermal ellipsoids with a probability of 30%; N–H···Cl contacts are shown by the dashed lines), (b) a supramolecular layer of $\{(neocH_2)^{2+}Cl\}_n$ chains (the dotted lines show N/C–H···Cl contacts), (c) a supramolecular layer of $\{(neocH_2)Cl\}_n$ chains and $AuCl_4^-$ anions (the dashed lines show N/C–H···Cl and Au···π contacts), (d) a supramolecular stack of $neocH^+$ cations (the dashed lines show π···π contacts; both protons on nitrogen atoms with a total population equal to 1 (see the experimental section) are shown here), and (e) and (f) projections of the crystal packing on the 0*ac* and 0*bc* planes, respectively (the dotted lines show N/C–H···Cl, Au–Cl···π, Au···π and π···π contacts); the blue and red outlines indicate stacks and layers, respectively.

coordinated DMSO/Cl complex. In the spectrum of complex **3**, already at the initial moment of time, two sets of signals are observed with a ratio of 10 : 1 from the initial complex (major set) and from the DMSO-substituted complex (presumably, $[Au(DMSO)_2(1,10\text{-phen})]^{3+}$ (**3′**)) (minor set) (Table S5 and Fig. S4, ESI†). The intensity of the signals of form **3** decreases over time, whereas that of form **3′** increases. After 144 h, form **3** is completely converted to form **3′**. A similar pattern is observed for **4**. The only difference is that complex **4** is even less stable in DMSO solution, and already at the initial time point, the DMSO complex ($[Au(bpy)(DMSO)_2]^{3+}$ (**4′**)) is present in solution in an amount comparable to that of **4** (Table S6 and Fig. S5, ESI†). The intensity of signals from **4′** increases with time. After 72 h, the signals from **4** disappear completely. Based on this study, we can conclude that in the case of complexes **1a**, **3** and **4**, the ^1H NMR spectra evolve over time, which is most likely a consequence of the reaction with the coordinating solvent (the replacement of Cl^- with DMSO). This is consistent with the fact that phenanthroline-like π-acceptor ligands have a strong *trans* effect, which enhances the lability of chloride ligands and facilitates Cl/DMSO exchange. For complexes **1** and **2a**, no spectral changes were detected up to 144 h, indicating either their stability in solution or a fast reaction with DMSO to give mixed DMSO/Cl species. In any case, reaction with DMSO does not affect the N-heterocycle; the formation of free ligands was not detected.

Table 1 Parameters of the D–H···A contacts in crystals of **1** and **2**

D–H···A	Symmetry equivalent	D–H, Å	H···A, Å	D···A, Å	D–H···A, deg.
1					
N1–H1···Cl1	$1+x, 1+y, z$	0.88	2.79	3.443(6)	132
N1–H1···N2	—	0.88	2.40	2.747(8)	104
N3–H3A···Cl9	—	0.88	2.15	3.033(6)	178
N3–H3A···N4		0.88	2.59	2.908(8)	102
N4–H4···Cl9		0.88	2.14	3.024(6)	177
N4–H4···N3		0.88	2.58	2.908(8)	103
C2–H2A···Cl8	$1+x, y, z$	0.95	2.75	3.650(8)	158
C16–H16···Cl6	$-x, -y, 1-z$	0.95	2.78	3.701(8)	163
C17–H17···Cl9	$x, -1+y, z$	0.95	2.70	3.578(8)	155
C25–H25···Cl9	$x, -1+y, z$	0.95	2.77	3.633(7)	151
C27–H27A···Cl9	$-x, 1-y, 1-z$	0.98	2.81	3.691(9)	149
2					
N1–H1···O3	$1-x, 2-y, 2-z$	0.82(4)	1.92(4)	2.727(4)	168(3)
N2–H2···O1	$1-x, 1-y, 1-z$	0.88	1.88	2.736(3)	163
C1–H1A···Cl2	$-x, 2-y, 2-z$	0.95	2.63	3.476(3)	148
C1–H1A···O2	$1-x, 2-y, 2-z$	0.95	2.54	3.188(4)	126
C6–H6···Cl4	$x, y, -1+z$	0.95	2.81	3.724(3)	162
C7–H7···Cl1	$1-x, 2-y, 1-z$	0.95	2.76	3.608(3)	148
C8–H8···O3	$1-x, 2-y, 2-z$	0.95	2.25	3.129(3)	154
C11–H11···Cl2	$-x, 1-y, 1-z$	0.95	2.73	3.469(3)	135
C12–H12···O2	$1-x, 1-y, 1-z$	0.95	2.41	3.328(3)	163

Table 2 X–Y···π interactions in crystals of **1** and **2**

Interaction	X···Cg_i[a], Å	H-Perp, Å	γ, deg.	Y–X···Cg_i, deg.	Y···Cg_i, Å
1					
Au2–Cl7···Cg_4	3.625(4)	3.420	19.39	109.07(8)	4.877(3)
Au2–Cl7···Cg_4	3.552(4)	3.492	10.55	98.40(8)	4.497(3)
Au2–Cl7···Cg_6	3.701(4)	3.409	22.91	70.21(7)	3.633(3)
Au2–Cl7···Cg_6	3.956(4)	3.511	27.44	60.99(6)	3.479(3)
Au2–Cl8···Cg_5	3.611(4)	3.562	9.45	92.61(8)	4.369(3)
Au2–Cl8···Cg_5	3.433(4)	3.361	11.74	92.59(8)	4.218(3)
2					
Au1–Cl1···Cg_2	3.4052(14)	3.396	4.17	119.66(3)	4.9481(13)
Au1–Cl2···Cg_1	3.7041(16)	3.259	28.37	154.22(3)	5.8386(14)
Au2–Cl3···Cg_1	3.5934(15)	3.409	18.42	108.16(3)	4.8232(13)
N3–O1···Cg_2	3.312(2)	2.912	28.46	80.58(14)	3.343(2)
N3–O1···Cg_3	2.995(2)	2.894	14.93	111.88(15)	3.647(2)
N3–O2···Cg_2	3.782(2)	3.739	8.67	59.97(13)	3.343(2)

[a] Cg_i is the centroid of a 6-membered ring [**1**: Cg_4 – N3C15–C19, Cg_5 – N4C20–C24, Cg_6 – C18C19C24C23C26C25; **2**: Cg_1 – N1C1–C5, Cg_2 – N2C6–C10, Cg_3 – C4C5C9C10C12C11]; H-Perp is the perpendicular distance from H to the ring; γ is the angle between the H → Cg vector and the normal to the ring plane.

Table 3 Selected parameters of π–π intermolecular interactions in **1**

$Cg_i\cdots Cg_j$	Symmetry index	Cg_i–Cg_j, Å	α, deg.	$Cg_{i\mathrm{Perp}}$, Å	Slippage, Å
$Cg_2\cdots Cg_2$	$-X, 1-Y, 2-Z$	3.844(4)	0	3.314(3)	1.947
$Cg_2\cdots Cg_2$	$1-X, 1-Y, 2-Z$	3.651(4)	0	3.332(3)	1.493
$Cg_2\cdots Cg_3$	$1-X, 1-Y, 2-Z$	3.600(4)	1.9(3)	3.318(3)	1.313

Studies in aqueous solutions

A comprehensive study of the behavior of the obtained compounds in aqueous solutions was carried out for complexes **1a** and **2a**. Similar studies for **3** and **4** were conducted earlier.[40,41,43] These complexes do not dissociate in aqueous solution, but with increasing pH, they are transformed from $AuLCl_2^+$ to $AuL(OH)_2^+$ (L = bipy or phen). Complexes **1** and **2** contain the $AuCl_4^-$ ion, which is stable only in the acidic region, and its reactions with thiols have already been reported.[38,39]

Determination of the protonation constants of neoc and 1,7-phen

Protonation equilibria were evaluated based on

$$A + H^+ \rightarrow HA^+, K_H \qquad (1)$$

where A = neoc or 1,7-phen, and were studied pH-metrically. During the experiments, aqueous solutions of neoc (3.0×10^{-4} M) or 1,7-phen (2.7×10^{-4} M) containing 0.2 M NaCl were titrated with HCl solution with the simultaneous measurement of pH (=$-\lg[H^+]$).

Experimental values of the formation function were calculated using $n^*_{exp} = (C_H - [H^+])/C_A$. Furthermore, $n^*_{calc} = K_H[H^+]/(1 + K_H[H^+])$. The protonation constants estimated using the nonlinear least squares method are log K_H = 5.60 (neoc) and 4.18 (1,7-phen). The values of n^*_{exp} and n^*_{calc} are shown in Fig. S6 (ESI†). The UV spectra of the ligands at pH 2.0 and 7.4 are shown in Fig. 3.

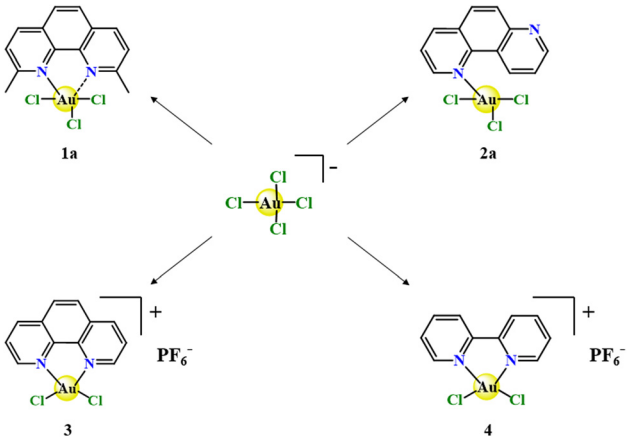

Scheme 2 Covalently bound fragments of oligopyridines forming Au(III) complexes.

Conductometric measurements

Even initial measurements (within 10 s of mixing) of the electrical conductivity of the solution containing the complex with neoc **1a** ($C_{Au} = 2.1 \times 10^{-4}$ M, 10% DMSO) showed that it is 6.1 times higher than the conductivity of NaCl solution at the same concentration. Subsequently, it changed little, *i.e.*, it increased by 6% in 1 h. This result indicates hydrolysis, which is consistent with previous qualitative conclusions[42] based on UV spectra. The first stage of hydrolysis leads to the appearance of two ions (H^+ and Cl^-) in the solution, and considering the abnormally high specific conductivity of H^+, the conductivity of such a solution should be 3.5 times higher than that of NaCl solution:

$$[Au(neoc)Cl_3] + H_2O \rightarrow [Au(neoc)Cl_2OH] + H^+ + Cl^- \qquad (2)$$

The measured conductivity shows that hydrolysis occurs further:

$$[Au(neoc)Cl_2OH] + H_2O \rightarrow [Au(neoc)Cl(OH)_2] + Cl^- + H^+, K_{2h} \qquad (3)$$

The value $[H^+] = 3 \times 10^{-4}$ M calculated from conductivity data is fully consistent with the measured pH of 3.5. From these data, the estimated log K_{2h} is −7.9. The analogous value for the second stage of $AuCl_4^-$ hydrolysis is −7.1.

For complex **2a** (with 1,7-phen), initial measurements of the electrical conductivity ($C_{Au} = 2 \times 10^{-4}$ M, 10% EtOH) showed

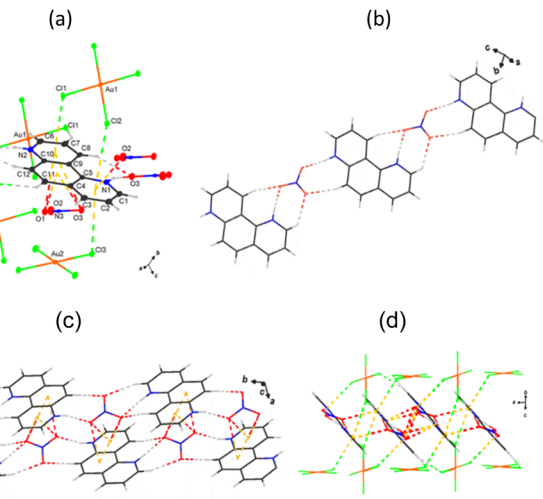

Fig. 2 Fragments of packing for **2**: (a) intermolecular interactions between the 1,7-phenH_2^{2+} dication and the $AuCl_4^-$ and NO_3^- anions (thermal ellipsoids with a probability of 30%, the dotted lines show N/C–H···O contacts), (b) the supramolecular chain {(1,7-phenH_2)NO_3} (the dotted lines show N/C–H···O and N–O···π contacts), (c) a fragment of a supramolecular layer of {(1,7-phenH_2)NO_3}$_n$ chains (dashed lines show N/C–H···O and N–O···π contacts), and (d) non-covalent interactions between {(1,7-phenH_2)NO_3}$_n$ layers and $AuCl_4^-$ anions (the dotted lines show N/C–H···O, C–H···Cl, N–O···π and Au–Cl···π interactions).

Scheme 3 The dynamic process in a solution of **1a**.

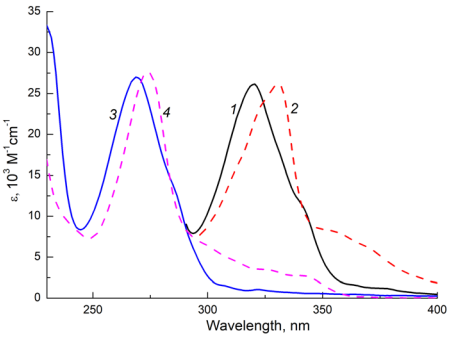

Fig. 3 UV spectra (molar absorptivities) of neoc (1), neocH$^+$ (2), 1,7-phen (3) and phenH$^+$ (4). For convenience, the spectra of neoc (1) and neocH$^+$ (2) are shifted to the right (towards higher wavelengths) by 50 nm. Spectra of neocH$^+$ (2) and phenH$^+$ (4) were obtained at pH 2.0, with those of neoc (1) and 1,7-phen (3) obtained at pH 7.4.

that it is 3.5 times higher than that of NaCl solution of the same concentration. Subsequently, it remained virtually unchanged. This is consistent with complete hydrolysis in the first step:

$$[Au(1,7\text{-phen})Cl_3] + H_2O \rightarrow [Au(1,7\text{-phen})(OH)Cl_2] + H^+ + Cl^-, \quad K_{1h} \quad (4)$$

Additional pH-metric measurements showed that if a solution contains complex **2a** ($C_{Au} = 5 \times 10^{-4}$ M) and 0.2 M NaCl, then its pH is 3.60 ($[H^+] = 2.6 \times 10^{-4}$ M). This means that hydrolysis is partially suppressed in the presence of NaCl. Titration with an alkali (NaOH) shows that within the first step ($C_{OH}/C_{Au} < 1$), equilibrium is attained rapidly, and then very slowly. That is, the system behaves similarly to $AuCl_4^-$. From pH measurements during titration, it follows that $\log K_{1h} = -4.4$ in the first step.

Stability of 1a in solution at pH 2.0 and 7.4

UV spectra of a solution containing complex **1a** at pH 2.0 ($C_{Au} = 5.06 \times 10^{-5}$ M, 0.2 M NaCl, 10% DMSO, $C_{HCl} = 0.01$ M) recorded immediately after preparation (15 s) and then again at 2 min and 20 min, showed no difference. Their shapes basically coincided with the spectrum of the free ligand at the same pH (Fig. 4a).

This means that under these conditions, complex **1a** decomposes very quickly, releasing free neocH$^+$ and transforming into $AuCl_4^-$. However, the decomposition of the obtained spectra into the contributions of these species, taking into account the absorption of DMSO (Fig. 4a), showed that if the calculated content of neocH$^+$ (4.6×10^{-5} M) is really close to the initial concentration of the complex, then the calculated concentration of $AuCl_4^-$ is two times lower. Probably, this is due to the reduction of gold(III) to $AuCl_2^-$.[42] This is possible because at low concentrations the following disproportionation equilibrium is shifted to the left:

$$3AuCl_2^- = 2Au^0 + AuCl_4^- + 2Cl^-, \lg K = 7.5$$

At a "physiological" pH of 7.4 in the presence of 0.2 M NaCl, the pattern is different. Complex **1a** also decomposes with the release of neoc (Fig. 4b), but this process occurs much more slowly.

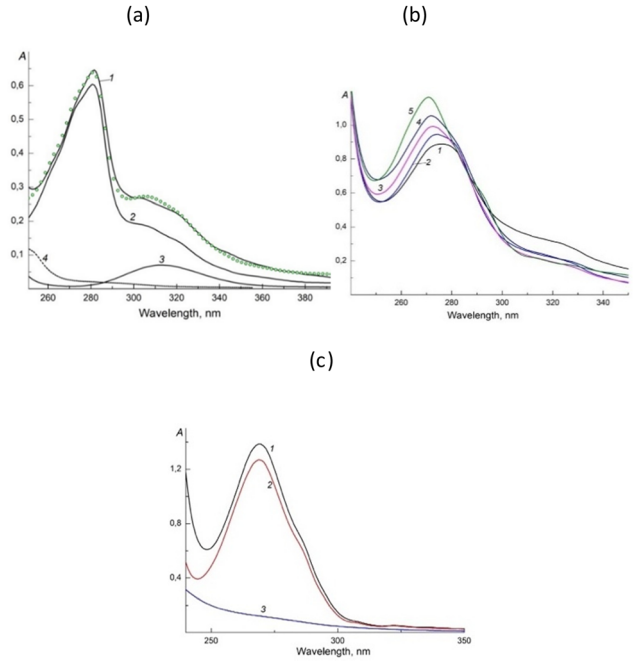

Fig. 4 (a) Decomposition of the UV spectrum of a solution of complex **1a** (1), recorded 20 min after preparation, into spectra of individual components; contributions: 2 – neocH$^+$, 3 – $AuCl_4^-$, and 4 – DMSO; circles – calculated spectrum (sum of 2 + 3 + 4); $C_{Au} = 5.06 \times 10^{-5}$ M, 0.2 M NaCl, pH 2.0, $l = 0.5$ cm. (b) Change over time of the UV spectrum of a solution of complex **1a** (pH 7.4): 10 s (1), 16 min (2), 41 min (3), 100 min (4), and 22 h (5); $C_{Au} = 7.6 \times 10^{-5}$ M, 0.2 M NaCl, $l = 0.5$ cm. (c) UV spectra of solutions: 1 – prepared from $[Au(1,7\text{-phen})Cl_3]$ (see main text); 2 – 1,7-phen; 3 – $AuCl_4$*; $C_{Au} = C_{phen} = 1.0 \times 10^{-4}$ M, pH 7.4, 0.2 M NaCl, $l = 0.5$ cm.

From the decomposition of the UV spectrum of the solution ($C_{Au} = 7.6 \times 10^{-5}$ M, 0.2 M NaCl, pH 7.4, $t = 25$ °C), recorded 22 h after its preparation, into the spectra of the components, it follows that 60% of neoc from the complex is released into solution. At the same time, a similar amount of $AuCl_4$* is formed – the equilibrium sum of gold(III) chloride-hydroxide complexes $[Au(OH)_iCl]_j$ – corresponding to the given pH. About 40% of the original complex remained undecomposed, and it may be a mixture of chloride-hydroxide species $[Au(neoc)(OH)_iCl_j]^+$, which have almost identical spectra.[39] This feature precludes the use of spectrophotometry for studying the substitution of Cl^- by OH^- in such complexes. Conversely, the fast decomposition of the complex upon the addition of an acid and the very low concentrations do not allow the use of conventional pH-metric analysis with acid titration for this purpose. However, if the concentration values obtained after 22 h are close to equilibrium, then the conditional constant (at pH 7.4 and $[Cl^-] = 0.2$ M) of the process

$$[Au(neoc)Cl_3]^* + Cl^- \rightarrow AuCl_4^* + neoc, K^* \quad (5)$$

is equal to $\log K^* = -3.5$, which is very close to the corresponding constant for pyridine,[43] which is not surprising considering the monodentate coordination of neoc with the Au(III) ion. Observations of the solutions were not extended beyond

one day, because traces of a precipitate appeared after that time.

Stability of 2a in solution at pH 2.0 and 7.4

As complex **2a** is poorly soluble in ordinary solvents and DMF absorbs strongly in the UV region,[11] an EtOH/DMSO mixture was used. However, these solvents also led to low solubility, especially if water was added. Moreover, complex **2a** exists in solution for only a short time. Upon a prolonged storage in solution or upon moderate heating (up to 50–60 °C to accelerate dissolution), **2a** decomposes with the release of the free ligand. Decomposition is promoted in the acidic region by protonation of 1,7-phen, while at higher pHs, it is driven by replacement with OH^-. In addition, decomposition is apparently favored by the low concentration due to poor solubility, as well as because of low stability due to the monodentate coordination of the ligand. For example, solutions with $C_{Au} = 5 \times 10^{-3}$ M can be prepared by dissolving the dry complex in DMSO. However, white particles appeared when this solution was used to prepare working solutions with $C_{Au} = 1 \times 10^{-4}$ M by adding water, buffer (pH 7.4) and NaCl. To dissolve them, the resulting solution was moderately heated for 40 min under stirring. Although the resulting solution was homogeneous, the UV spectrum showed that it no longer contained the original complex, but only free 1,7-phen and $AuCl_4^-$ (Fig. 4c).

Interaction with GSH

Glutathione (GSH) is one of the most common intracellular metabolites (along with thioredoxin reductase and topoisomerase), the concentration of which in cancer cells is 0.5–10 mM.[44] This thiol causes the reduction of gold(III) to gold(I), accompanied by the formation of a highly stable gold(I) thiolate complex[39,45] and the release of the free ligand, which, in turn, is also often capable of exhibiting biological activity. In an acidic medium, complex **1a** is immediately converted to $neocH^+$ and $AuCl_4^-$.[39] As it was intended to use complexes studied in biological experiments, the study was carried out at pH 7.4, with a GSH concentration characteristic of cytoplasm (1×10^{-3} M) and in the presence of 0.2 M NaCl. At a permissible concentration C_{Au} of 10^{-5} M, GSH is present in excess, and bis-thiolate $[Au(GSH)_2]^{3-}$ with protonated amino groups and deprotonated carboxyl groups is the only possible gold(I) complex under these conditions.[39,45] When gold(III) is reduced, GSH is oxidized to its disulfide form (GSSG) if present in excess, or to sulfinic or sulfonic acids in other cases. For complexes **1a** and **2a**, the pattern of transformation was very similar (Fig. 5).

For example, at pH 7.4, complex **1a** was rapidly ($\tau < 10$ s, indistinguishable in our experiments) converted to $[Au(GSH)_2]^{3-}$ (Fig. 6). The resulting spectrum was decomposed into the known spectra of the components, and their calculated concentrations were found to be close to those expected for quantitative conversion: $[Au(GSH)_2]^{3-} = 4.8 \times 10^{-5}$ M and $[neoc] = 5.2 \times 10^{-5}$ M at an initial $C_{Au} = 5.0 \times 10^{-5}$ M. The standard deviation for the fitted data in Fig. 6 was 0.007, which is close to the error in determining the absorption *A*. Complex **2a** also reacts rapidly with excess GSH with the quantitative reduction of gold(III) to $[Au(GSH)_2]^{3-}$ and the release of free 1,7-phen.

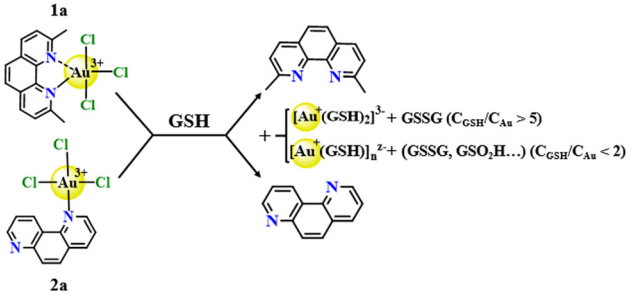

Fig. 5 Interaction of Au(III) complexes **1a** and **2a** with GSH.

At $C_{GSH} = 2.0 \times 10^{-3}$ M and $C_{Au} = 9.0 \times 10^{-5}$ M, the reaction is completed in less than 20 s, after which the spectrum of the solution does not change. At lower GSH concentrations, the process proceeds somewhat more slowly and leads, in addition to $[Au(GSH)_2]^{3-}$, to the formation of the highly stable polymeric complex $(AuGSH)_n$. However, on the whole, the spectrum of the solution remains almost identical to that of free 1,7-phen.

Although complexes **3** and **4** are completely stable against decomposition in aqueous solution, they also react rapidly with GSH under similar conditions (pH 7.4, 0.2 M NaCl).[40,41] The process results in the reduction of gold(III) to gold(I) with the formation of highly stable gold(I) thiolates. Two examples are shown in Fig. S7 (ESI†) for $C_{GSH}/C_{Au} = 5/1$. After only 10 s, the residue of the starting complex is about 10%; after 1 min, the reaction is complete.

Thus, the study shows that complexes **1a** and **2a** are unstable in aqueous solutions; they undergo hydrolysis (reactions (1)–(4)) and rapidly (in an acid medium) or slowly (at pH 7.4) eliminate the N-donor ligand, turning into mixed forms $[Au(OH)_iCl_j]^-$. This is due to the monodentate (**2a**) or pseudo-monodentate coordination (**1a**) of the heterocycle with the Au(III) ion.

In contrast, complexes **3** and **4** with bidentate-coordinated 1,10-phen and bpy are stable in solution. The only process is ligand substitution: at pH 7.4, Cl^- ions are replaced by OH^- ions to give $[Au(1,10\text{-phen})(OH)_2]^+$ or $[Au(bpy)(OH)_2]^+$. However,

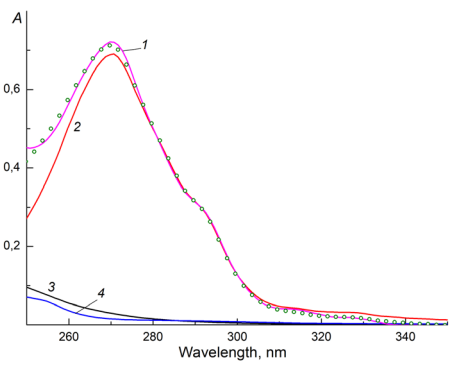

Fig. 6 Decomposition of the UV spectrum of a solution of complex **1a** (1), recorded 10 minutes after mixing with GSH, into spectra of individual components; contributions: 2 – $neocH^+$, 3 – $[Au(GSH)_2]^{3-}$, and 4 – DMSO; circles – the calculated spectrum (sum of 2 + 3 + 4); $C_{Au} = 5.0 \times 10^{-5}$ M, $C_{GSH} = 2.0 \times 10^{-3}$ M, pH 7.4, 0.2 M NaCl.

Table 4 Cytotoxicity (IC_{50} ± SD, μM) of the compounds against human solid cell lines and normal fibroblasts after 72 h[a]

	IC_{50}				SI^b		
Compound	HCT116	A549	SKBR3	HDF	HCT116	A549	SKBR3
1	0.0017 ± 0.0004	0.8 ± 0.4	3.5 ± 1.6	0.63 ± 0.16	371.0	0.8	0.2
1a	0.21 ± 0.05	2.6 ± 1.2	2.0 ± 0.6	35.6 ± 2.5	169.6	13.7	17.8
2	89 ± 3	130 ± 40	112 ± 11	228 ± 14	2.6	1.7	2.0
Cisplatin	7.7 ± 0.5	5 ± 0.3	7.9 ± 0.6	23 ± 2	2.9	4.6	2.9

[a] Experiments were performed in triplicate (n = 3). [b] SI = IC_{50} for non-cancer cells/IC_{50} for cancer cells.

all complexes (**1a**, **2a**, **3** and **4**) rapidly react with GSH under near-physiological conditions to give gold(I) thiolate complexes, in particular, $[Au(GSH)_2]^{3-}$. This is facilitated by the presence of Cl^- or OH^- ions capable of rapid replacement by a nucleophile of GS^- type, the high redox potential of gold(III) complexes, and the very high stability of gold(I) thiolate complexes.

Biological activity

The study of biological activity considered the differences in the structures of the complexes: (non)coordinated/(non)chelated N-donor ligands.

Cytotoxic properties of 1, 1a and 2

The inhibitory potential of the compounds was assayed by using the 3-(4,5-dimethylthiazol-2-yl)-2,5-diphenyltetrazolium bromide (MTT) assay against three cell lines, including human breast adenocarcinoma (SKBR3), human colorectal adenocarcinoma (HCT116) and human lung carcinoma (A549). The IC_{50} values for the tested compounds are presented in Table 4. Cytotoxic selectivity was evaluated using a non-tumor culture of human dermal fibroblasts (HDF). The SI (selectivity index) was calculated by the formula: IC_{50} (non-cancer cells)/IC_{50} (cancer cells). In our study, compound **2** (Fig. 7) showed a moderate cytotoxic effect in the studied concentration range against human colorectal carcinoma cells HCT116, as evidenced by the IC_{50} value of 88.87 ± 3.23 μM. Regarding the other two lines, A549 and SKBR3, the compound was weakly active with IC_{50} values >100 μM. On the contrary, compounds **1** and **1a** exhibited a higher level of cytotoxic activity compared to the reference drug ($p < 0.05$), with active concentrations ranging from the nanomolar to submicromolar level in the case of the HCT116 line (IC_{50}: 1.7 ± 0.04 nM (**1**); 0.21 ± 0.05 μM (**1a**)) and at the micromolar level in the case of SKBR3 and A549 cells: 2.0 ± 0.56 μM and 2.60 ± 1.18 μM, respectively, for **1a** (Table 4). The effects of the complexes on various cancer lines are presented in Fig. 8.

It should also be noted that a high level of selective activity was shown by **1a** (Table 4), as revealed in relation to a non-cancerous culture of human fibroblasts; the SI values were 17.8, 13.7 and 169.6 in comparison with the cancer cell lines SKBR3, A549, and HCT116, respectively. It should be noted that for complex **1**, the SI in relation to human colorectal carcinoma cells (HCT116) was highest (371.0). The revealed effectiveness and selectivity of compounds **1** and **1a** allows us to consider them as the most promising compounds for anticancer therapy.

Antimycobacterial activity

The antibacterial activities of compounds **1–3** were determined *in vitro* against a non-pathogenic *M. smegmatis* strain and

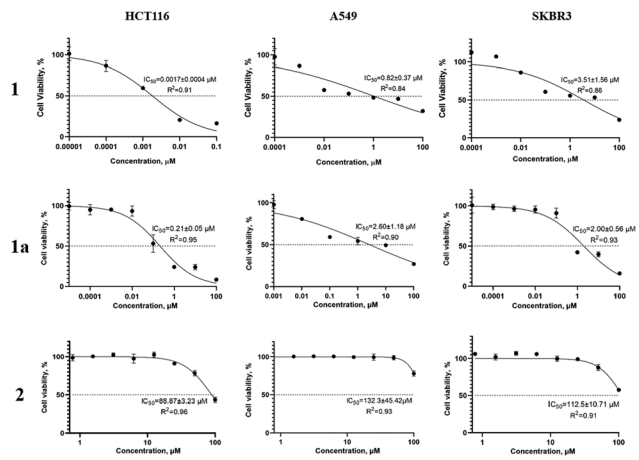

Fig. 7 The antiproliferative activities of **1**, **1a** and **2** against sensitive human tumor cell lines *in vitro* (incubation time: 72 h).

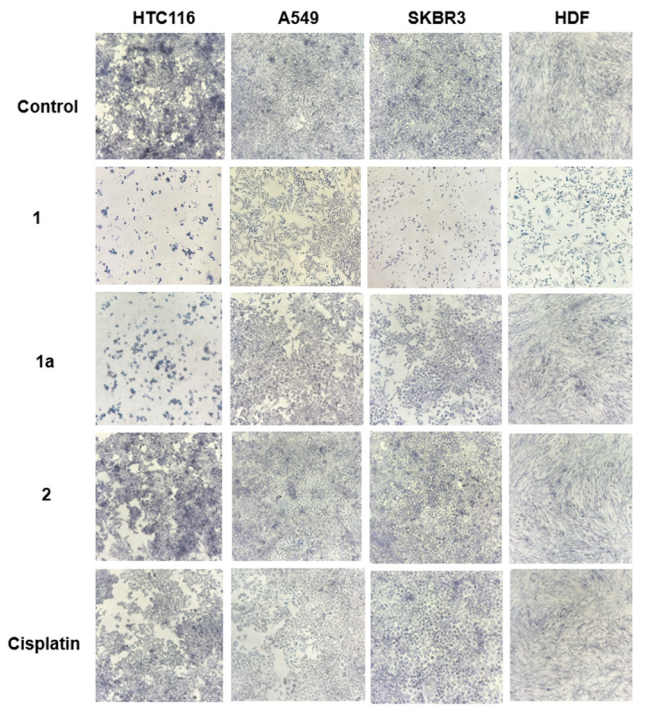

Fig. 8 Cytotoxic effects of complexes **1**, **1a** and **2** on various cell lines in comparison with an intact control (MTT staining, ×100).

Table 5 The results of antibacterial activity against *M. smegmatis*

Compound	MIC, nmol per disk	The zone of inhibition, mm	
	24 h	24 h	120 h
1	20	6.8 ± 0.6	6.3 ± 0.3
1a	25	6.8 ± 0.3	6.2 ± 0.1
2	100	6.5 ± 0.1[b]	0
2a	20	6.5 ± 0.1	6.1 ± 0.1
3	20	6.6 ± 0.3	6.2 ± 0.2
$H[AuCl_4]$	2	6.4 ± 0.0[b]	0
$Na[AuCl_4]$	2	6.4 ± 0.0[b]	0
bpy[3]	500	0	0
neoc[3]	100	6.50 ± 0.06[b]	0
1,10-phen[28]	45	6.50 ± 0.06[b]	0
1,7-phen	200	6.5 ± 0.4	6.1 ± 0.1
Rif	5	6.9 ± 0.5[a]	6.9 ± 0.4[a]
INH	100	7.0 ± 0.5	6.5 ± 0.5

The diameter of the paper disk is 6 mm. [a] The zone of inhibition of culture growth does not overgrow within the specified time. [b] The zone of inhibition of growth of the bacterial culture, which initially appeared after several hours of growth, begins to show overgrowth for the entire surface of the zone.0: no growth inhibition zone.

virulent *M. tuberculosis H37Rv*. It is known that the resistance of mycobacteria to chemotherapeutic agents is due to the low permeability of their cell wall, which has an unusual structure. *M. smegmatis* are fast-growing, non-pathogenic bacteria and are therefore used as model organisms for the slow-growing *M. tuberculosis* in the primary screening of antituberculosis drugs.[46] The *M. smegmatis* test system exhibits a higher degree of resistance to antibiotics and antituberculosis agents than *M. tuberculosis*, therefore the selection criterion is a compound concentration of <100 nmol per disc, in contrast to *M. tuberculosis* (MIC < 2 μg mL^{-1}).[47] All the results obtained relating to the *in vitro* bioactivity of the compounds studied were compared to the activity of isoniazid (INH) and rifampicin (Rif), *i.e.*, the first-line drugs for tuberculosis treatment, under these experimental conditions. The concentration of the compound at which the minimum visible zone of growth inhibition is observed is considered as the MIC (minimum inhibitory concentration, nmol per disc). Inhibition zone analysis is carried out after 24 h and after 120 h (Table 5), which allows us to obtain important information about the effects of the test substance on the mycobacterial culture. Analysis after five days allows us to assess the effects the test substance has on mycobacteria: either they die completely (bactericidal effect) or their growth slows down but does not stop completely (bacteriostatic effect). The biological activities of individual (free) Hfur against *M. smegmatis* are comparable to that of INH (Table 5), but this effect persists for only one day. The results showing antibacterial activity in the *M. smegmatis* test system and the variation over time for compounds **1–3** are shown in Table 5. As follows from the data displayed in Table 5, complexes **1**, **1a**, **2a** and **3** exhibit efficient bioactivity (nearly the same for all the compounds). Complex **2** is an exception, featuring a MIC significantly higher than those of the other compounds. The measured activities of $Na[AuCl_4]$ and $H[AuCl_4]$ showed lower MIC values (and were therefore more efficient) compared with the reference drug Rif. However, the growth inhibition zone almost was almost immediately overgrown, indicating that these compounds cannot be considered effective against the mycobacterial strain. Conversely, the MIC values of the free oligopyridine ligands (Table 5) are higher than those of the corresponding complexes. This implies that upon complex formation, both the efficiency of the chelate complex and the time of effect toward the strain increase. For complexes **1** and **1a**, antibacterial activity was measured against the *M. tuberculosis H37Rv* strain that is sensitive to all antituberculosis drugs (Table 6). As *M. tuberculosis* is slow-growing bacteria, the MICs of the test compounds are determined based on microdilution in the liquid nutrient medium. Table 6 shows that complex **1a** exhibits greater antibacterial activity against Mtb than **1** (MICs: 12.5 and 25 μg L^{-1}, respectively).

Table 6 The results of antibacterial activity against *M. tuberculosis H37Rv*

Compound	MIC, μg mL^{-1}
1	25
1a	12.5
INH	0.03

Molecular docking and molecular dynamics studies on 1

Simulations of molecular interactions of proteins with the ligand (neoc) and complex **1** were carried out using AutoDock software 4.2.6.[48] The procedure protocol and simulation techniques are given in the Experimental section. As a result of docking, five stable protein-neocuproin complexes were obtained. They are presented in Table 7.

The stability metric of the resulting complexes was the zero value of the root mean square deviation of atoms (RMSD). To visualize the bonds formed between active-site amino acids and the N-ligand, protein.pdb and ligand.pdb files were exported to PyMOL. As a result, images of complexes with highlighted bonds were created, as shown in Fig. 9. Of all the complexes, the complex of neocuproin with MSMEG_0615 (ATPase, AAA family protein, T7SS_EccA) showed the highest affinity. Ligand docking with the ABC-type multidrug transport systems MSMEG_6553 (ABC transporter ATP-binding protein, MdlB) and MSMEG_6554 (ABC transporter ATP-binding protein, ViuB/MdlB) formed two complexes each, but with a minimal difference in binding energy. The above data indicate that neocuproin is capable of forming stable complexes with low conformational variability with *M. smegmatis* proteins. The results of docking seven *M. smegmatis* proteins with the Au^{3+}

Table 7 The successful conformations and binding energies of protein-neoc supramolecular complexes

Protein	Quantity of successful complexes (number of successful conformations)	Binding energy, kcal mol^{-1}
MSMEG_0615	1 (41)	−5.81
MSMEG_6553	2 (20, 100)	−4.56
		−4.47
MSMEG_6554	2 (55, 52)	−4.49
		−4.26

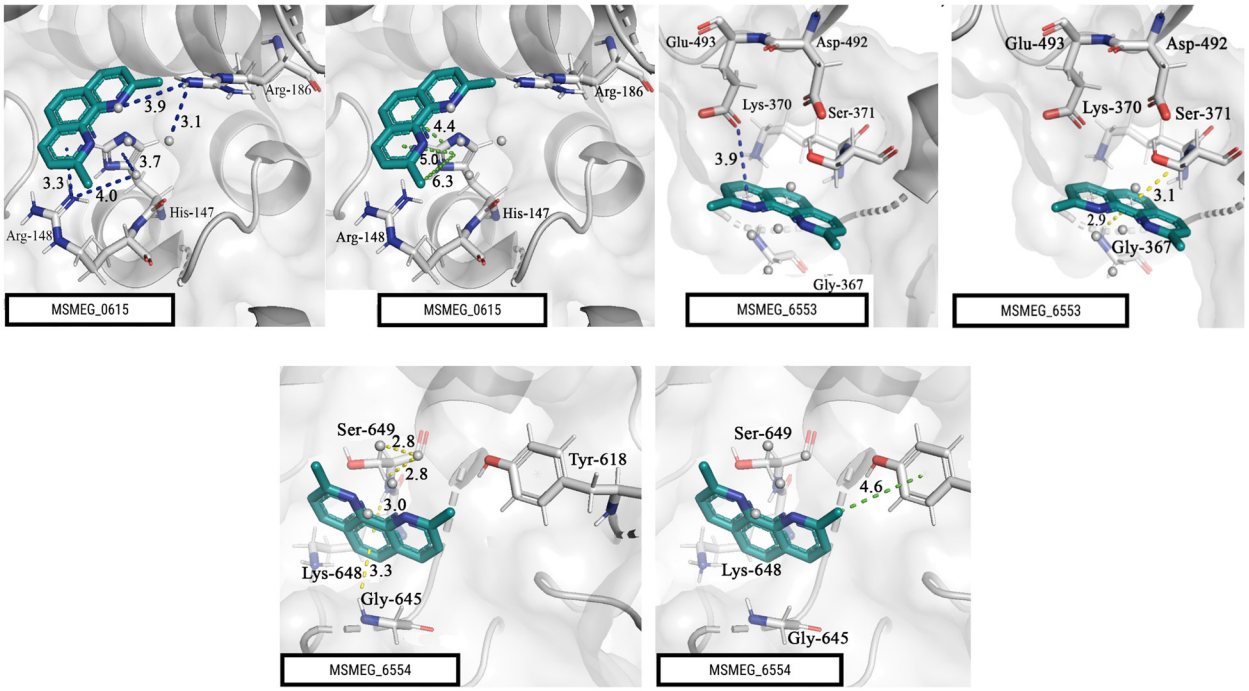

Fig. 9 Images of the resulting protein-neocuproin complexes (MSMEG_0615, MSMEG_6553 20th conformation, and MSMEG_6554 55th conformation) with highlighted bonds (hydrogen – yellow, electrostatic – blue, and hydrophobic – green).

center in **1** as well as the molecular dynamics results are presented in Table 8. (The output data of the energy minimization procedures, NVT and NPT ensembles, are in accordance with the tolerance limits established by the protocol.) Plots of the RMSD of protein backbone atoms (Fig. S8, ESI†) show that all proteins lose structural integrity over time upon interaction with Au^{3+} ions, which is reflected in an RMSD increase to values of 3^{-10} Å. This fact suggests that gold(III) ions, as representative heavy metals, are capable of triggering the unfolding of proteins, which can affect their ligand-binding abilities, and as a consequence, their direct functions. Another interesting result was that after a ten-nanosecond simulation, all gold ions remained bound to the protein. Analysis of the three complexes given in Table 9 and the clear example of the MSMEG_0615 complex (Fig. 10) showed the following: (1) almost all Au^{3+} ions are bound through hydroxyl (O–H) and/or carbonyl (C═O) oxygen atoms within glutamic and aspartic acids, although one of theinteractions (in MSMEG_6553) occurs through the histidine N atom; and (2) all types of Au···O and Au···N interactions are in the range of ∼2.8–3.4 Å. Based on the

Table 8 Amino-acid residues of *M. smegmatis* proteins predicted by the MIB2 server that are capable of forming supramolecular complexes with the Au^{3+} ion of **1** and intermediate values for the stages of balancing dynamic protein systems (all values are averaged over the entire system)

No.	*M. smegmatis* locus tag	Score	Most likely amino acids	Other potential amino acids	Minimum potential energy of the system, kJ mol^{-1}	Temperature in the system (NVT ensemble), K	System pressure (NPT ensemble), bar	System pressure (subsequent NPT ensembles, N),[a] bar
1	MSMEG_0615	8.680 6.048 5.192 3.258 2.477	62C, 63D	62C, 63D 404Q, 405H 6A, 10R 8C, 9C, 74Q	$-1.13689 \times 10^{+6}$	299.562	−3.09502	0.959741(2)
2	MSMEG_6553	6.356 5.208 4.884	416L, 462G	561E, 565R 560D, 564R	$-4.30923 \times 10^{+6}$	299.582	−3.58487	0.256888(2)
3	MSMEG_6554	3.533 6.365 5.693 4.467 4.078	729M, 730R	91H, 92 E 126P, 403H 407T, 408H 179V, 180H	$-3.51252 \times 10^{+6}$	299.658	−5.61381	0.250072(3)

[a] Provided that during the first 2 ns of the simulation the system did not reach the reference value of $0 < \rho < 2$ bar.

Table 9 Au^{3+}-binding clusters in *M. smegmatis* proteins and their corresponding bond lengths

System	Complex composition		Corresponding bond lengths, Å	Number of connections in the complex	Model relevance[a]
	No.	Amino acids			
MSMEG_0615	1	Asp269, Asp272, Glu274	1.4; 2.8; 3.4	6	Au^{3+}, n = 6, octahedral
	2	Asp89, Glu114	1.4; 3.2; 3.4	4	Au^{3+}, n = 4, planar
	3	Glu127	1.4	2	—
	4	Glu224, Glu227	1.4; 3.3	4	Au^{3+}, n = 4, planar
	5	Asp170	1.4; 3.1	2	—
MSMEG_6553	1	Asp87, His91	1.3; 1.4; **3.2**[b]	3	—
	2	Asp182, Asp186, Glu298	1.4; 3.1–3.4	6	Au^{3+}, n = 6, octahedral
	3	Asp508	1.3; 1.4	2	—
	4	Glu568, Asp571	1.4; 3.3; 3.4	4	Au^{3+}, n = 4, planar
MSMEG_6554	1	Asp521	1.4	2	—
	2	Glu598	1.3; 3.2	2	—
	3	Asp717, Asp721	1.4; 3.4	3	—
	4	Glu770	1.4	2	—
	5	Asp776, Glu778	1.3; 2.9; 3.3	3	—

– = no identical data. [a] Relevance analysis was carried out according to data from the WebElements website (**https://winter.group.shef.ac.uk/webelements/gold/atom_sizes.html**). [b] The bond formed with the N of histidine is highlighted in bold.

results of the analysis of ion-binding protein clusters, five of all the clusters studied match the reference values based on the number of bond lengths. It is not possible to assess the reliability of the existence of the clusters found using molecular dynamics simulation data using CHARMM36m, as this force field does not consider the polarizability properties of its components (amino-acid residues, K^+, Cl^-, Au^{3+}, water molecules) but only simulates their pairwise interactions with fixed point charges (for example, the point charge of AU3P in CHARMM36m is 3.000 and does not change upon interaction), even though such interactions are fundamental in such systems.[49] Nevertheless, these data are the first to be reported in the scientific literature, which gives them some value for future research and establishes a conditional basis that may be confirmed or refuted in the future.

Conclusions

New ionic complexes of gold(III)-containing protonated oligopyridines, **1** and **2**, have been prepared from strongly acidic solutions. Protonation of N-donor ligands, which was found to block their ability to form covalent/coordination bonds with the metal centre, results in the formation of ionic complexes (in contrast to non-acidic solutions where direct coordination

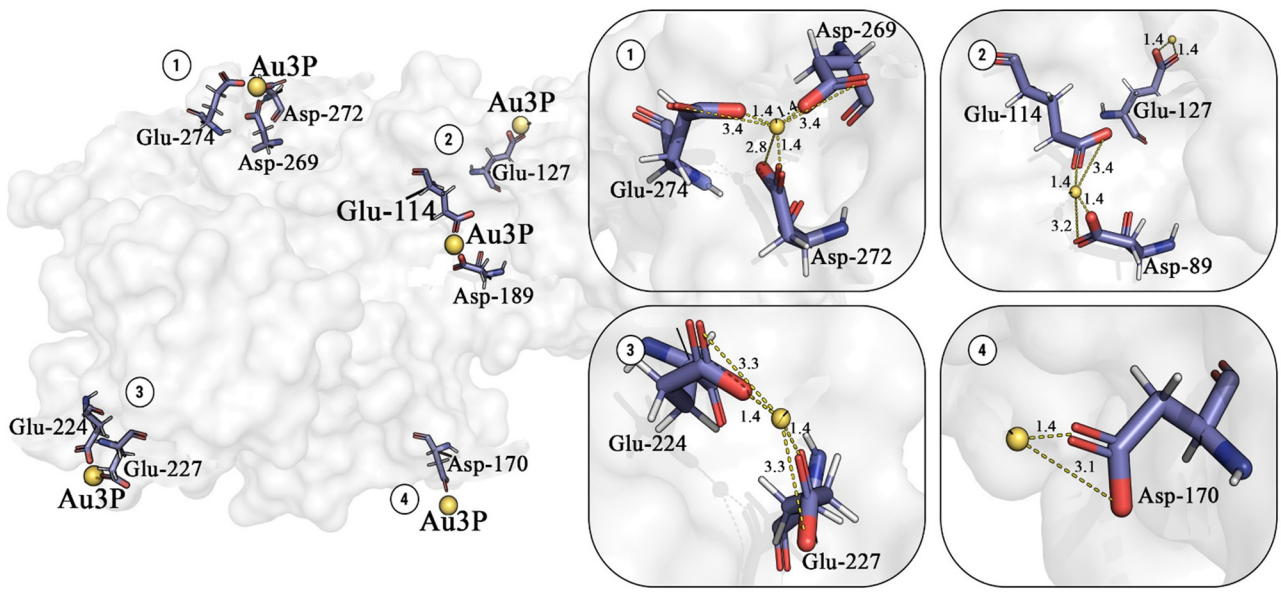

Fig. 10 The MSMEG_0615 complex with different types of ion-binding clusters (clusters 2 and 3 are combined).

between phenanthroline or bipyridine moieties and gold(III) is observed, *i.e.*, complexes **1a**, **2a**, **3** and **4**).

A study of the hydrolytic stability of **1a**, **2a**, **3** and **4** showed that the dissociation rate of the N-donor ligand is determined by its type of coordination with the Au(III) ion and the pH of the medium: bidentate-coordinated **3** and **4** are completely stable, while monocoordinated **1a** and **2a** are unstable. However, complexes **1a**, **2a**, **3** and **4** all quickly react with GSH under near-physiological conditions, forming gold(I) thiolate complexes, in particular, $[Au(GSH)_2]^{3-}$. This process is facilitated by the presence of Cl^-/OH^- ligands, which can be quickly replaced by a GS^{3-}-type nucleophile; the high redox potential of gold(III) complexes; and, most importantly, the very high stability of gold(I) thiolate complexes. Results from *in vitro* biological testing using a non-pathogenic *M. smegmatis* strain showed higher efficiency for chelated oligopyridine moieties; however, they did not reveal any fundamental differences related to the type of complex. The cytostatic activities of **1** and **1a** significantly exceed that of cisplatin while simultaneously exhibiting high selectivity index values, indicating the high potential of those compounds. In contrast to **1** and **1a**, the antiproliferative activity of complex **2**, containing a monodentate-linked 1,7-phenanthroline moiety, is low, and the compound is more toxic to healthy fibroblasts. After conducting molecular docking studies between complex **1** and neocuproine, the formation of stable neocuproine–protein and **1**–protein supramolecular associates was observed, which indicates their high affinity for the target proteins. Molecular dynamics simulations showed that gold(III) ions can cause the unfolding of proteins, disrupting their native structure and deteriorating their functional properties.

Experimental

A solution of $H[AuCl_4]$ in aqua regia (hydrochloric acid (reagent grade, Khimmed) and nitric acid (65%, reagent grade, Khimmed)) with a gold concentration of 3 mg mL^{-1} was used for the synthesis of complexes **1** and **2**. Complexes **1** and **2** were synthesized in air using distilled water, 1,7-phenanthroline (98%, Acros), neocuproine (98%, Aldrich), and acetonitrile (special purity grade, Khimmed). Complexes $[Au(neoc)Cl_3]$ (**1a**), $[Au(1,7\text{-phen})Cl_3]$ (**2a**), $[Au(1,10\text{-phen})Cl_2]PF_6$ (**3**) and $[Au(bpy)Cl_2]PF_6$ (**4**) were prepared as described in the literature.[11,30–32] Their purity was confirmed by elemental analysis and NMR spectroscopy (Fig. S9–S12, ESI†). NaCl, NaOH, DMSO and ethanol were used as purchased. Phosphate buffer (pH = 7.4) was prepared from a pH-metric standard (pH = 6.86) by adding NaOH. Preparation of aqueous solutions was as follows. Initial solutions of the complex (usually 5.0×10^{-3} M) were prepared by dissolving a sample of **1a** or **2a** in DMSO (special grade). Aliquots were taken from these solutions to prepare working aqueous solutions. The concentration of DMSO in these solutions was 10%. In all cases, except for conductometric measurements, the solutions contained 0.2 M NaCl. The pH of working solutions was adjusted by adding either HCl (pH = 2.00) or phosphate buffer (C_{pb} = 0.01 M).

Physical measurements

IR spectra were recorded in the 400–4000 cm^{-1} region using a Spectrum-65 PerkinElmer FT-IR spectrometer. Microprobe analyses were carried out using a Carlo Erba EA 1108 Series CHN elemental analyser; for the analysis of metals we used a mass spectrometric method with inductively coupled plasma (ICP-MS) (Agilent 7500 ce; Agilent Technologies Inc., USA) (Center of Collective Use of IGIC RAS).

^1H NMR spectra (500 MHz) were acquired on a Bruker Avance-500 spectrometer with a 5-mm PABBO-PLUS probe at room temperature. The chemical shifts were given in parts per million (ppm) from tetramethylsilane. The UV absorption spectra of solutions were recorded on an SF 2000 spectrophotometer in the wavelength range of 250–400 nm with l = 0.2–2 cm, and the reference solution was water. Identification of reaction products was carried out using known UV spectra of possible components. The resulting spectra were decomposed into the spectra of components using multiple regression.[39] The electrical conductivity of the solutions was measured using a Radelkis OK 102/1 conductometer. The cell constant was determined from measurements in aqueous solutions of NaCl at 298 K. The pH of solutions was measured using a Radelkis OP-208 pH meter. The glass combined electrode ESK 10301/7 was calibrated using HCl solutions in 0.2 M NaCl; the measured pH values were in the form $-\lg[H^+]$.

Synthesis of 1 and 2

$\{(neocH_2)[AuCl_4]\}_2 \cdot Cl$ (**1**): a weighed amount of neoc (0.18 g, 1 mmol) was dissolved in MeCN (20 mL). A solution (2 mL) of $H[AuCl_4]$ (in HCl/HNO_3) was added to the resulting solution, and the mixture was continuously stirred for 40 min (60 °C). The solution was filtered and allowed to evaporate at room temperature. After 24 h, straw-colored crystals were formed; the crystals were separated from the mother liquor by decantation and dried in air. The yield of 1 was 0.25 g (76%).

$C_{28}H_{27}Cl_9N_4Au_2$: calculated: C 29.69; H 2.40; N 4.95%; found: C 29.82; H 2.39; N 5.02%.

IR (ATR; ν, cm^{-1}): 3360 w, 3204 w, 3060 w, 2918 w, 2603 w, 2555 w, 2422 w, 1992 w, 1911 w, 1821 m, 1757 w, 1678 s, 1626 s, 1600 m, 1531 w, 1500 w, 1408 m, 1329 m, 1222 s, 1153 m, 1094 m, 1035 s, 1125 m, 956 s, 864 s, 832 s, 802 w, 762 w, 708 w, 678 w, 630 w, 540 s, 412 m.

$(1,7\text{-phen}H_2)[AuCl_4] \cdot NO_3$ (**2**): a weighed amount of 1,7-phen (0.18 g, 1 mmol) was dissolved in MeCN (20 mL). A solution (2 mL) of $H[AuCl_4]$ (in HCl/HNO_3) was added to the resulting solution, and the mixture was continuously stirred for 40 min (60 °C). The solution was filtered and allowed to evaporate at room temperature. After 24 h, straw-colored crystals were formed; the crystals were separated from the mother liquor by decantation and dried in air. The yield of 2 was 0.23 g (69%).

$C_{12}H_{10}Cl_4N_3Au$: calculated: C 21.01; H 1.01; N 14.01%; found: C 21.12; H 1.03; N 14.08%.

IR (ATR; ν, cm^{-1}): 3116 w, 3040 w, 2808 w, 2093 w, 2010 w, 1642 m, 1620 m, 1598 m, 1550 m, 1501 w, 1413 s, 1315 s, 1284 s, 1236 s, 1088 w, 1028 m, 950 w, 885 w, 837 s, 795 w, 769 s, 709 s, 616 m, 589 w, 552 w, 522 w, 487 w, 455 w, 422 w, 405 w.

Single crystal X-ray analysis

An experimental array of reflection was obtained by the standard method on Bruker SMART APEX II (for **1**) and Bruker D8 Venture (for **2**) diffractometers equipped with a CCD detector and a monochromatic radiation source (MoKα radiation, λ = 0.71073 Å). Semiempirical absorption correction for both samples was applied using SADABS software.[50] Using Olex2 software[51] the structure was solved with ShelXT[52] and refined with the olex2.refine[50] refinement package, with least-squares minimisation against F^2 in an anisotropic approximation for non-hydrogen atoms. The structures of **1** and **2** were solved by a direct method and refined using the full-matrix anisotropic approximation for all non-hydrogen atoms using Olex2 software. Hydrogen atoms of the carbon-containing ligands were geometrically generated and refined in the riding model. The solution for structure **1** was obtained considering the monoprotonated form of the 1,10-phenanthroline molecule, in which the hydrogen atoms at N1 and N2 are located with occupancies of 0.82(11) and 0.18(11), respectively.

Biological activity

Cell culture and cytotoxicity assays. A panel of human solid tumor cell lines was used in the *in vitro* study. Breast adenocarcinoma (SKBR3, HTB-30), colorectal adenocarcinoma (HCT116, CCL-247) and lung carcinoma (A549, CCL185) samples were obtained from the American Type Culture Collection (ATCC, Rockville, MD) with short tandem repeat-based authentications and mycoplasma-free status. Cytotoxic selectivity was evaluated using a non-tumor culture of human dermal fibroblasts (HDF, lonza, CC-2511). Cells were grown in RPMI-1640 medium (Gibco, UK) supplied with 10% FBS (fetal bovine serum, HyClone/Cytiva, USA) and 1% penicillin/streptomycin and incubated at 37 °C with 5% CO_2. The cells were seeded in a 96-well sterile plate (3-6 × 10^3 cells per well) and kept overnight at 37 °C in 95% humidity supplied with 5% CO_2. Series of different concentrations of compounds were prepared with DMSO and serum-free medium and added to the cells. The maximum concentration of DMSO in the investigations was <1.5%, and this demonstrated no cell lethality. The cells were co-incubated with the compounds for 72 h. Next, 20 μL of MTT staining reagent (5 mg mL^{-1} in a phosphate cradle arrangement) was added to each well, and the plates were incubated at 37 °C for additional time. After 4 h of incubation, the supernatant was removed and 200 μL of dimethyl sulfoxide (DMSO) was added to each well to solubilize the formazan crystals, and absorbance was recorded at 540 nm using a microplate reader (Multiscan FC, Thermo Fisher Scientific). Untreated cells were run in each assay as the negative control group. Cisplatin was chosen as a reference drug. All the experiments were performed in triplicate (n = 3). The IC_{50} values were calculated based on nonlinear regression curves using GraphPad Prism version 9.0 for Windows. The results were analysed using one-way ANOVA with Tukey's multiple comparison test using SPSS 21 software and were accepted as significantly different when $p <$ 0.05 (Table S7, ESI†). IC_{50} data are presented as mean ± standard deviation (SD).

Antimycobacterial activity of 1–3. To determine the biological activities of complexes **1–3** and whether they possessed antiproliferative properties in the *Mycobacterium smegmatis mc² 155* test system, the paper disk-diffusion method was used. The technique involved determining the size of the zone of inhibition of the growth of the strain, seeded as a lawn on an agar medium, around paper disks containing the compounds in various concentrations. Bacteria washed off Petri dishes with Trypton-soy agar M-290 medium (Himedia) were grown overnight in Lemco-TW liquid medium (Lab Lemco Powder: 5 g L^{-1} (Oxoid), Peptone special: 5 g L^{-1} (Oxoid), NaCl: 5 g L^{-1}, and Tween-80) at 37 °C until the average logarithmic growth phase at an optical density OD_{600} was 1.5, then they were mixed with molten agar medium M-290 at a ratio of 1 : 9 : 10 (culture : Lemco-TW : M-290), and the resulting mixture was poured as a top layer onto Petri dishes (5 mL per dish) with already solidified M-290 agar medium. After the agar in the top layer solidified, paper disks soaked with a solution of the test substance were placed on the plate surface. The culture was incubated for 24 h at 37 °C. The diameter of the zone of inhibition of *M. smegmatis* growth around the paper disk impregnated with the compound was determined. The MIC (minimum inhibitory concentration) was taken as the concentration of the compound where the zone of growth inhibition was the smallest.

Antituberculosis activity

A study of the antimycobacterial activities of the compounds was carried out based on the REMA method.[53,54] A suspension of Mtb with 1.0 McFarland turbidity was prepared (using saline) from a culture of *Mycobacterium tuberculosis H37Rv* in the logarithmic phase of growth on Löwenstein-Jensen medium. An Mtb suspension at a concentration of 3 × 10^8 CFU per mL (50 μL) was transferred into a tube with Middlebrook 7H9 nutrient broth and OADC growth supplement. The resulting suspension (100 μL) was added to the wells of the plates.

Preparation of dilutions of the test compounds: dilutions of the test compounds were prepared using DMSO and sterile distilled water (isoniazid was dissolved only in water). Weighed portions of the compounds to be tested were dissolved in the calculated volume of DMSO in such a way as to obtain a stock solution with a concentration of 1666.7 μg mL^{-1}. Further, a two-fold dilution was carried out using pure DMSO. In this way, solutions were obtained (in DMSO) with the following concentrations of complexes **1** and **1a**: 833.3, 416.7, 208.3, 104.2, 52.1, 26.0, and 13.0 μg mL^{-1}.

Evaluating procedure: for testing compounds, culture medium (97 μL) and solutions of the test complexes (3 μL) prepared as described above were added to the wells of a 96-well plate. Then, Mtb suspension (100 μL) was added to the wells of the plates. Thus, the following concentrations of tested complexes were obtained in the wells of the plate: 25, 12.5, 6.25, 3.13, 1.56, 0.78, 0.39, and 0.20 μg mL^{-1}. The DMSO concentration in all wells is 1.5 (vol%). As a positive control, Mtb culture was used without adding complexes and with the addition of DMSO (final concentration: 1.5%). Isoniazid was used as a reference drug. The plates were incubated at 37 °C for 7 day. After the incubation time, 30 μL of resazurin solution (with the addition of Tween 80) was added to the wells, and incubation was continued at 37 °C. The results were recorded after 24, 48,

and 72 h. The minimal inhibitory concentration (MIC) was taken as the minimum concentration of test compound that prevents the colour change of resazurin.

In silica studies

Preparation of protein structures. The selection of proteins in pdb format for the bacterium *M. smegmatis* was carried out using the RCSB-PDB database (PDB ID: 7NAZ, locus tag: MSMEG_0615) and AlphaFold DB (AlphaFold ID: A0R6H7, locus tag: MSMEG_6553; AlphaFold ID: A0R6H8, locus tag MSMEG_6554). The following proteins were chosen as model proteins: ESX-3 secretion system protein EccA3, locus_tag: MSMEG_0615; Mycobactin import ATP-binding/permease protein IrtB, locus_tag: MSMEG_6553; Mycobactin import ATP-binding/permease protein IrtA, (locus_tag: MSMEG_6554). These proteins were selected from 13 proposed options because they have the highest degree of evidence of existence (at the protein level). Before molecular docking, energy minimization procedures for all protein structures were performed utilizing the CHARMM36m[55] force field with the GROMACS 2024 software package. Prediction of the molecular pockets of selected proteins was carried out using the PrankWeb web service.[56–58]

Molecular docking of neocuproin with proteins in AutoDock 4.2. Modeling of the molecular interactions of proteins with ligands was carried out using AutoDock 4.2.6 software.[48] The protocol for the procedure consisted of several stages: preparation of the target protein and ligand, creation of a grid (docking area), and docking.pdb (protein) and .pdbqt (ligand) format files containing data on the coordinates of atoms and their charges were imported into the program. Protein preparation involved removing water molecules and various inclusions (MSMEG_0615), protonating polar amino acids, and calculating partial atomic charges. This experiment used Kollman charges, which are calculated using the AMBER force field and are based on the electron density in the molecular orbit. This type of charge is considered the most accurate and suitable for the preparation of large biopolymers. Ligand preparation involved automatic detection of the torsion tree. Next came the process of applying the mesh. The protein.pdb file was converted to .pdbqt format for further meshing. The highest speed data obtained as a result of using the PrankWeb service was used as the coordinates of the docking area. The grid size and spacing were set as standard ($40 \times 40 \times 40$ points and 0.375 Å, respectively), as the predicted molecular pockets of the target proteins fit completely within the grid. After importing the grid overlay coordinates in.gpf format, the AutoGrid program, which is included in AutoDock 4.2.6 software, was launched. Upon completion of the program,.map and .maps files were created, which contain information about the coordinates of the overlaid grid. After obtaining the protein structure with a superimposed network, the molecular docking preparation stage followed. The parameters of the genetic algorithm were selected to carry out 100 iterations and export information in.dpf format, after which the AutoDock program included in AutoDock 4.2.6 software was launched. After docking, the ligands of successful complexes were exported in.pdb format for visualization.

Molecular docking of Au^{3+} with proteins in MIB2. The affinity of Au^{3+} ions for *M. smegmatis* proteins was assessed by the method of rigid intermolecular docking on the MIB2 web server,[59] which allows for the prediction of amino acid residues with ions. The result of the calculations is the prediction of amino acid residues that can form complexes with the metal ion and the ranking of possible complexes (score value).

Molecular dynamics of protein–Au^{3+} complexes. In order to evaluate the results of predictions from MIB2, as well as to test the ability of Au^{3+} ions to have an inhibitory effect on proteins while remaining bound to them, we carried out molecular dynamics simulations of protein–Au^{+} complexes (PDB ID: 7NAZ; AlphaFold IDs: A0R6H7, A0R6H8) with the parameterization of atoms by the widely used CHARMM36m force field[55] in the GROMACS 2024 software package (package compiled locally using the CUDA 12 single-precision library).[60] Before preparing the molecular dynamics system, individual chains for each gold atom were added to the MIB2 PDB files of the complexes. Mdp files of the minimization procedure, NVT, NPT ensembles and MD simulations were considering the specifics of the force field.

The preparation of simulation domain topology files was carried out using the CHARMM-GUI web service[61] with standard settings in an explicit solvent (TIP3P water model). Each system was equilibrated with K^+ and Cl^- ions at a standard concentration of 0.15 mM, and the appropriate amounts of potassium and chlorine ions were added to the simulation area and distributed using the Monte Carlo method. Gold atoms (AU) were reparametrized to Au^{3+} (AU3P). Due to the fact that the system is a dynamic ensemble of atoms that change their positions over time, in the protein complex A0R6H7 (MSMEG_6553) one of the gold atoms was removed because it merged with another and was located at a negligible distance from it. The procedure for minimizing the energy of the system was carried out using a steep descent method until it reached its minimum ($n_{steps} = -1$). In the NVT ensemble, temperature baths of protein atoms and gold atoms were combined and set to 300 K using a V-rescale thermostat, and the system was simulated for 1 ns in 2 fs steps. In the NPT ensemble, the system pressure was controlled isotropically at 1 bar using a C-rescale barostat for 2 ns in 2 fs steps. If the average system pressure did not reach a value close to 1 bar (no less than 0 bar, no more than 2 bar), an additional NPT ensemble was simulated using a Nose–Hoover barostat[62] for 0.5 ns with the same periodicity; the temperature in the ensemble was distributed between two baths: (1) protein atoms with Au^{3+}; and (2) water atoms and K^+ and Cl^- ions. In all simulations using the LINCS method,[63] restrictions were imposed on all types of connections. The near electrostatic and van der Waals cut-offs were set at 1.2 nm (CHARMM specific). Electrostatic interactions were calculated using the particle mesh Ewald method with an offset of 0.15 nm. Each stage of system balancing was controlled using the built-in 'gmx energy' utility. Due to the fact that gold ions interact with the protein predominantly electrostatically, and there is no open literature data on potential interactions of amino acids with Au^{3+}, the analysis of bond-length parameters was carried out based on the final coordinates of the complexes

(t = 10 000 ps) using the 'Wizard Measurement' tool (measurement mode: polar neighbours in other objects) in the PyMOL v. 3.0.0 software package. (The PyMOL Molecular Graphics System, Version 3.0.0, Schrödinger, LLC). All resulting clusters were further evaluated for the relevance of their ion-binding ability, based on the coordination number of bonds potentially formed with the Au(III) gold ion. The characteristic values of coordination numbers (n) for Au^{3+} are 4 and 6 with planar and octahedral symmetry types, respectively. To visualize the complexes, the PyMOL v. 3.0.0 program was used. Analysis of simulation data and the plotting of data were carried out in a Jupyter Notebook using the NumPy, Pandas and Plt.plot libraries.

Author contributions

The manuscript was written through contributions from all authors. I. A. Lutsenko, I. L. Eremenko, A. L. Gushchin – scientific idea, writing the manuscript, supervision – review & editing. K. A. Koshenskova, E. E. Bardina – synthesis. E. V. Makotchenko, V. Yu. Kharlamova – studies in aqueous solutions. I. V. Mironov – interaction with GSH. M. A. Kiskin – X-ray analysis, writing the manuscript. O. B. Bekker – studies of antimycobacterial activity. E. M. Treschalina, D. V. Sokolova, V. S. Pokrovsky – cell culture and cytotoxicity assays. E. A. Borodin, D. D. Kotelnikov, N. Yu. Leusova – molecular docking of neocuproin with proteins in AutoDock 4.2. E. A. Timofeev – molecular docking of Au^{3+} with proteins in MIB2. D. V. Belyaev, D. V. Vakhrusheva, S. Yu. Krasnoborova, G. L. Rusinov – studies of antituberculosis activity, writing the paper.

Conflicts of interest

There are no conflicts to declare.

Data availability

The data supporting this article have been included as part of the ESI.† The main crystallographic data and refinement parameters for **1** and **2** are given in Table S1 (ESI†). Assignment of signals in the ^{1}H NMR spectra are given in Tables S2–S6 and Fig. S1–S5 (ESI†). Formation functions for the protonation of neoc and phen are given in Fig. S6 (ESI†). UV spectra of the reactions of $Au(bipy)(OH)_2^+$ and $Au(phen)(OH)_2^+$ with GSH are shown in Fig. S7 (ESI†). Graphs of the standard deviations for the complexes MSMEG_0615, MSMEG_6553, MSMEG_6554 are given in Fig. S8 (ESI†). CHN analysis and NMR spectra for **1a**, **2a**, **3** and **4** are given in Fig. S9–S12 (ESI†).

Acknowledgements

This research was funded by the Russian Science Foundation (project no. 22-13-00175-P). We are grateful to the User Facilities Center of Institute of General and Inorganic Chemistry of the Russian Academy of Sciences and the Centre of Collective Usage of Nikolaev Institute of Inorganic Chemistry SB RAS for physicochemical measurements. Physicochemical studies in solutions were carried out with the support of the Ministry of Science and Higher Education of Russia as part of the state assignment of NIIC SB RAS. Biological experiments were supported by the state program of the Ministry of Science and Higher Education of the Russian Federation (075-01551-23-00; FSSF-2023-0006).

Notes and references

1 N. P. E. Barry and P. J. Sadler, *Chem. Commun.*, 2013, **49**, 5106–5131.
2 U. Ndagi, N. Mhlongo and M. E. Soliman, *Drug Des., Dev. Ther.*, 2017, **11**, 599–616.
3 I. A. Lutsenko, D. E. Baravikov, K. A. Koshenskova, M. A. Kiskin, Y. V. Nelyubina, P. V. Primakov, Y. K. Voronina, V. V. Garaeva, D. A. Aleshin, T. M. Aliev, V. N. Danilenko, O. B. Bekker and I. L. Eremenko, *RSC Adv.*, 2022, **12**, 5173–5183.
4 M. A. Uvarova, D. E. Baravikov, F. M. Dolgushin, T. M. Aliev, K. O. Titov, O. B. Bekker, A. I. Lashkin, I. K. Malyants, V. O. Shender, M. A. Kiskin, I. L. Eremenko and I. A. Lutsenko, *Inorg. Chim. Acta*, 2023, **556**, 121649.
5 A. Climova, E. Pivovarova, M. Szczesio, K. Gobis, D. Ziembicka, A. Korga-Plewko, J. Kubik, M. Iwan, M. Antos-Bielska, M. Krzyżowska and A. Czylkowska, *J. Inorg. Biochem.*, 2022, **240**, 112108.
6 G. B. Kauffman, *Gold Bull.*, 1985, **18**, 31–44.
7 S. Mahdihassan, *Am. J. Chin. Med.*, 1985, **13**, 93–108.
8 B. Glišić and M. I. Djuran, *J. Chem. Soc., Dalton Trans.*, 2014, **43**, 5950–5969.
9 B. Warzajtis, B. D. Glišić, N. D. Savić, A. Pavic, S. Vojnovic, A. Veselinović, J. Nikodinovic-Runic, U. Rychlewska and M. I. Djuran, *Dalton Trans.*, 2017, **46**, 2594–2608.
10 J. J. Zhang, R. W. Y. Sun and C. M. Che, *Chem. Commun.*, 2012, **48**, 3388–3390.
11 A. Pavic, B. Glišić, S. Vojnovic, B. Warżajtis, N. D. Savić, M. Antić, S. Radenković, G. V. Janjić, J. Nikodinovic-Runic, U. Rychlewska and M. I. Djuran, *J. Inorg. Biochem.*, 2017, **174**, 156–168.
12 C. G. Hartinger, S. Zorbas-Seifried, M. A. Jakupec, B. Kynast, H. Zorbas and B. K. Keppler, *J. Inorg. Biochem.*, 2006, **100**, 891–904.
13 F. Lentz, A. Drescher, A. Lindauer, M. Henke, R. A. Hilger, C. G. Hartinger, M. E. Scheulen, C. Dittrich, B. K. Keppler and U. Jaehde, *Anticancer. Drugs*, 2009, **20**, 97–103.
14 R. V. Parish and S. M. Cottrill, *Gold Bull.*, 1987, **20**, 3–12.
15 G. D. Hoke, R. A. Macia, P. C. Meunier, P. J. Bugelski, C. K. Mirabelli, G. F. Rush and W. D. Matthews, *Toxicol. Appl. Pharmacol.*, 1989, **100**, 293–306.
16 G. D. Hoke, G. F. Rush, G. E. Bossard, J. V. McArdle, B. D. Jensen and C. K. Mirabelli, *J. Biol. Chem.*, 1988, **263**, 11203–11210.
17 M. J. McKeage, S. J. Berners-Price, P. Galettis, R. J. Bowen, W. Brouwer, L. Ding, L. Zhuang and B. C. Baguley, *Cancer Chemother. Pharmacol.*, 2000, **46**, 343–350.

18 S. J. Berners-Price and P. J. Sadler, *Coord. Chem. Rev.*, 1988, **46**, 27–102.
19 J. Carlos Lima and L. Rodriguez, *Adv. Anticancer Agents Med. Chem.*, 2012, **11**, 921–928.
20 S. J. Berners-Price, C. K. Mirabelli, R. K. Johnson, M. R. Mattern, F. L. McCabe, L. F. Faucette, C. M. Sung, S. M. Mong, P. J. Sadler and S. T. Crooke, *Cancer Res.*, 1986, **46**, 5486–5493.
21 C. K. Mirabelli, D. T. Hill, L. F. Faucette, F. L. McCabe, G. R. Girard, D. B. Bryan, B. M. Sutton, J. O. Leary Barus, S. T. Crooke and R. K. Johnson, *J. Med. Chem.*, 1987, **30**, 2181.
22 P. F. Smith, G. D. Hoke, D. W. Alberts, P. J. Bugelski, S. Lupo, C. K. Mirabelli and G. F. Rush, *J. Pharmacol. Exp. Ther.*, 1989, **249**, 944–950.
23 G. Marcon, S. Carotti, M. Coronnello, L. Messori, E. Mini, P. Orioli, T. Mazzei, M. A. Cinellu and G. Minghetti, *J. Med. Chem.*, 2002, **45**, 1672–1677.
24 L. Messori, F. Abbate, G. Marcon, P. Orioli, M. Fontani, E. Mini, T. Mazzei, S. Carotti, T. O'Connell and P. Zanello, *J. Med. Chem.*, 2000, **43**, 3541–3548.
25 P. Calamai, S. Carotti, A. Guerri, T. Mazzei, L. Messori, E. Mini, P. Orioli and G. P. Speroni, *Anticancer Drug Des.*, 1998, **13**, 67–80.
26 L. L. F. Maciel, W. R. de Freitas, E. S. Bull, C. Fernandes, A. Horn, J. C. de Aquino Almeida and M. M. Kanashiro, *J. Inorg. Biochem.*, 2020, **210**, 111166.
27 I. A. Lutsenko, M. E. Nikiforova, K. A. Koshenskova, M. A. Kiskin, Y. V. Nelyubina, P. V. Primakov, M. V. Fedin, O. B. Becker, V. O. Shender, I. K. Malyants and I. L. Eremenko, *Russ. J. Coord. Chem.*, 2021, **47**, 881–890.
28 K. A. Koshenskova, D. E. Baravikov, L. A. Kayukova, E. M. Ergalieva, Y. V. Nelyubina, M. E. Nikiforova, F. M. Dolgushin, M. V. Fedin, O. B. Bekker, V. O. Shender, I. K. Malyants, T. M. Aliev, K. O. Titov, I. L. Eremenko and I. A. Lutsenko, *Polyhedron*, 2024, **251**, 116852.
29 T. Zou, C. T. Lum, C. N. Lok, J. J. Zhang and C. M. Che, *Chem. Soc. Rev.*, 2015, **44**, 8786–8801.
30 W. T. Robinson and E. Sinn, *J. Chem. Soc., Dalton Trans.*, 1975, 726–731.
31 A. Casini, M. C. Diawara, R. Scopelliti, S. M. Zakeeruddin, M. Grätzel and P. J. Dyson, *J. Chem. Soc., Dalton Trans.*, 2010, **39**, 2239–2245.
32 R. E. Ferraz De Paiva, D. H. Nakahata and P. P. Corbi, *Acta Crystallogr., Sect. E: Crystallogr. Commun.*, 2017, **73**, 1048–1051.
33 I. A. Lutsenko, O. V. Loseva, A. V. Ivanov, I. K. Malyants, V. O. Shender, M. A. Kiskin and I. L. Eremenko, *Russ. J. Coord. Chem.*, 2022, **48**, 808–812.
34 M. A. Cinellu, L. Maiore, M. Manassero, A. Casini, M. Arca, H. H. Fiebig, G. Kelter, E. Michelucci, G. Pieraccini, C. Gabbiani and L. Messori, *ACS Med. Chem. Lett.*, 2010, **1**, 336–339.
35 G. Gorini, F. Magherini, T. Fiaschi, L. Massai, M. Becatti, A. Modesti, L. Messori and T. Gamberi, *Biomedicines*, 2021, **9**, 871.
36 V. Volarevic, M. Milovanovic, A. Djekovic, Ž. D. Bugarcic and N. Arsenijevic, *Serb. J. Exp. Clin. Res.*, 2012, **13**, 99–102.
37 N. Y. Shmelev, T. H. Okubazghi, P. A. Abramov, M. I. Rakhmanova, A. S. Novikov, M. N. Sokolov and A. L. Gushchin, *Cryst. Growth Des.*, 2022, **22**, 3882–3895.
38 I. V. Mironov and E. V. Makotchenko, *J. Solution Chem.*, 2009, **38**, 725–737.
39 I. V. Mironov and V. Y. Kharlamova, *Inorg. Chim. Acta*, 2021, **525**, 120500.
40 I. V. Mironov and V. Y. Kharlamova, *Russ. J. Inorg. Chem.*, 2022, **67**, 1051–1057.
41 I. V. Mironov, V. Y. Kharlamova and J. Hu, *Russ. J. Inorg. Chem.*, 2023, **68**, 287–293.
42 Z. D. Hudson, C. D. Sanghvi, M. A. Rhine, J. J. Ng, S. D. Bunge, K. I. Hardcastle, M. R. Saadein, C. E. MacBeth and J. F. Eichler, *Dalton Trans.*, 2009, 7473–7480.
43 I. V. Mironov and L. D. Tsvelodutf, *Zh. Neorg. Khim.*, 2001, **46**, 154–159.
44 V. I. Lushchak, *J. Amino Acids*, 2012, **2012**, 1–26.
45 I. V. Mironov and V. Y. Kharlamova, *J. Solution Chem.*, 2020, **49**, 583–597.
46 S. Ramón-García, C. Ng, H. Anderson, J. D. Chao, X. Zheng, T. Pfeifer, Y. Av-Gay, M. Roberge and C. J. Thompson, *Antimicrob. Agents Chemother.*, 2011, **55**, 3861–3869.
47 O. B. Bekker, D. N. Sokolov, O. A. Luzina, N. I. Komarova, Y. V. Gatilov, S. N. Andreevskaya, T. G. Smirnova, D. A. Maslov, L. N. Chernousova, N. F. Salakhutdinov and V. N. Danilenko, *Med. Chem. Res.*, 2015, **24**, 2926–2938.
48 G. M. Morris, H. Ruth, W. Lindstrom, M. F. Sanner, R. K. Belew, D. S. Goodsell and A. J. Olson, *J. Comput. Chem.*, 2009, **30**, 2785–2791.
49 L. X. Phan, V. C. Chamorro, H. Martinez-Seara, J. Crain, M. S. P. Sansom and S. J. Tucker, *Biophys. J.*, 2023, **122**, 1548–1556.
50 L. Krause, R. Herbst-Irmer, G. M. Sheldrick and D. Stalke, *J. Appl. Crystallogr.*, 2015, **48**, 3–10.
51 O. V. Dolomanov, L. J. Bourhis, R. J. Gildea, J. A. K. Howard and H. Puschmann, *J. Appl. Crystallogr.*, 2009, **42**, 339–341.
52 G. M. Sheldrick, *Acta Crystallogr., Sect. C: Struct. Chem.*, 2015, **71**, 3–8.
53 J. C. Palomino, A. Martin, M. Camacho, H. Guerra, J. Swings and F. Portaels, *Antimicrob. Agents Chemother.*, 2002, **46**, 2720–2722.
54 N. K. Taneja and J. S. Tyagi, *J. Antimicrob. Chemother.*, 2007, **60**, 288–293.
55 J. Huang, S. Rauscher, G. Nawrocki, T. Ran, M. Feig, B. L. De Groot, H. Grubmüller and A. D. MacKerell, *Nat. Methods*, 2016, **14**, 71–73.
56 D. Jakubec, P. Skoda, R. Krivak, M. Novotny and D. Hoksza, *Nucleic Acids Res.*, 2022, **50**, W593–W597.
57 L. Jendele, R. Krivak, P. Skoda, M. Novotny and D. Hoksza, *Nucleic Acids Res.*, 2019, **47**, W345–W349.
58 R. Krivák and D. Hoksza, *J. Cheminf.*, 2018, **10**, 1–12.
59 C. H. Lu, C. C. Chen, C. S. Yu, Y. Y. Liu, J. J. Liu, S. T. Wei and Y. F. Lin, *Bioinformatics*, 2022, **38**, 4428–4429.
60 M. J. Abraham, T. Murtola, R. Schulz, S. Páll, J. C. Smith, B. Hess and E. Lindah, *SoftwareX*, 2015, **1–2**, 19–25.
61 S. Jo, T. Kim, V. G. Iyer and W. Im, *J. Comput. Chem.*, 2008, **29**, 1859–1865.
62 D. J. Evans and B. L. Holian, *J. Chem. Phys.*, 1985, **83**, 4069–4074.
63 B. Hess, H. Bekker, H. J. C. Berendsen and J. G. E. M. Fraaije, *J. Comput. Chem.*, 1997, **18**, 1463–1472.

